J. Space Weather Space Clim. 3 (2013) A08
DOI: 10.1051/swsc/2013031

SWSC

RESEARCH ARTICLE OPEN ACCESS

Geomagnetic activity during the rising phase of solar cycle 24

Ian G. Richardson*

CRESST and Department of Astronomy, University of Maryland, College Park, and The Astroparticle Physics Laboratory, Code 661, NASA Goddard Space Flight Center, Greenbelt, Maryland
*Corresponding author: e-mail: ian.g.richardson@nasa.gov

Received 4 January 2013 / Accepted 16 February 2013

ABSTRACT

As previous studies have shown, geomagnetic activity during the solar minimum following solar cycle 23 was at low levels unprecedented during the space era, and even since the beginning of the K_p index in 1932. Here, we summarize the characteristics of geomagnetic activity during the first 4 years of cycle 24 following smoothed sunspot minimum in December, 2008, and compare these with those of similar periods during earlier cycles going back to the start of K_p (cycles 17–23). The most outstanding feature is the continuing low levels of geomagnetic activity that are well below those observed during the rising phases of the other cycles studied. Even 4 years into cycle 24, geomagnetic storm rates are still only comparable to or below the rates observed during activity *minima* in previous cycles. We note that the storm rate during the rising phases of cycles 17–23 was correlated with the peak sunspot number (SSN) in the cycle. Extrapolating these results to the low storm rates in cycle 24 suggests values of the peak SSN in cycle 24 that are consistent with the NOAA Space Weather Prediction Center prediction of 90 ± 10, indicating that cycle 24 is likely to be the weakest cycle since at least 1932. No severe ($Dst < -200$ nT) storms have been observed during the first 4 years of cycle 24 compared with 4 in the comparable interval of cycle 23, and only 10 intense ($Dst < -100$ nT) storms, compared with 21 in cycle 23. These storms were all associated with the passage of Interplanetary Coronal Mass Ejections (ICMEs) and/or their associated sheaths. The lack of strong southward magnetic fields in ICMEs and their sheaths, their lower speeds close to the average solar wind speed, a ~20% reduction in the number of ICMEs passing the Earth, and weaker than normal fields in corotating high-speed streams, contribute to the low levels of geomagnetic storm activity in the rise phase of cycle 24. However, the observation of an ICME with strong southward fields at the STEREO A spacecraft on July 24, 2012, which would have been highly geoeffective had it encountered the Earth, demonstrates that strong geomagnetic storms may still occur during weak solar cycles.

Key words. interplanetary coronal mass ejection (CME) – Solar cycle – stream – Solar activity – interplanetary medium

1. Introduction

As is well established, geomagnetic activity, as measured by indices such as K_p (Menvielle & Berthelier 1991) and Dst (Sugiura 1964), is principally driven by the plasma and magnetic field conditions in the solar wind that encounters the Earth (e.g., Hirshberg & Colburn 1969; Arnoldy 1971; Tsurutani & Gonzalez 1997; O'Brien & McPherron 2000; Ji et al. 2010; and references therein). As proposed by Dungey (1961), the interaction between the solar wind and the Earth's magnetic field is strongest when the interplanetary magnetic field (IMF) has a southward component and hence is in the opposite direction to the Earth's dipolar magnetic field, facilitating reconnection between the IMF and the Earth's magnetic field at the dayside magnetopause. One parameterization of the solar wind energy input into the magnetosphere is the ε parameter (Perrealt & Akasofu 1978) given by $\varepsilon = l_0^2 V_{sw} B^2 \sin^4(\theta/2)$, where l_0^2 is the area of the magnetopause through which the energy enters, V_{SW} is the solar wind speed, B is the magnetic field intensity, and θ is the "clock angle" of the IMF relative to the Sun-Earth line; ε has the form of the Poynting flux in the upstream solar wind. Thus, geomagnetic activity reflects conditions in the solar wind that encounters the Earth which in turn are influenced by both long-term changes and transient activity at the Sun (e.g., Russell 1975; Feynman & Crooker 1978; Stamper et al. 1999; Richardson et al. 2000, 2002a, 2002b; Svalgaard & Cliver 2010; Richardson & Cane 2012a; and references therein).

Several studies (e.g., Russell et al. 2010; Tsurutani et al. 2011; Richardson & Cane 2012a, 2012b) have noted that geomagnetic activity during the minimum following solar cycle 23 was exceptionally low, and associated with unusual solar wind conditions, in particular low magnetic field intensities unprecedented during the space era, and slow flow speeds. In this paper, we summarize the characteristics of geomagnetic activity and the solar wind drivers during the first 4 years of solar cycle 24 following smoothed sunspot minimum in December 2008. In particular, we point out that geomagnetic activity continued to be at exceptionally low levels during the rise phase of cycle 24 compared to similar intervals in cycles 17 (the first full cycle for which the K_p index is available) to 23, and discuss the contributing factors.

2. Geomagnetic activity during the first 4 years of cycles 17–24

The top panel of Figure 1 shows the yearly mean sunspot number (SSN) since 1932, the start of the K_p geomagnetic index, covering the late decline of solar cycle 16 to the rise phase of cycle 24. Red vertical lines indicate years with minimum SSN, while black lines indicate the year of peak SSN in each cycle. The lower panel shows the number of days ("storm days") in each year when geomagnetic activity was at the NOAA G1 ("minor storm") level; the NOAA storm levels are described at http://www.swpc.noaa.gov/NOAAscales/.

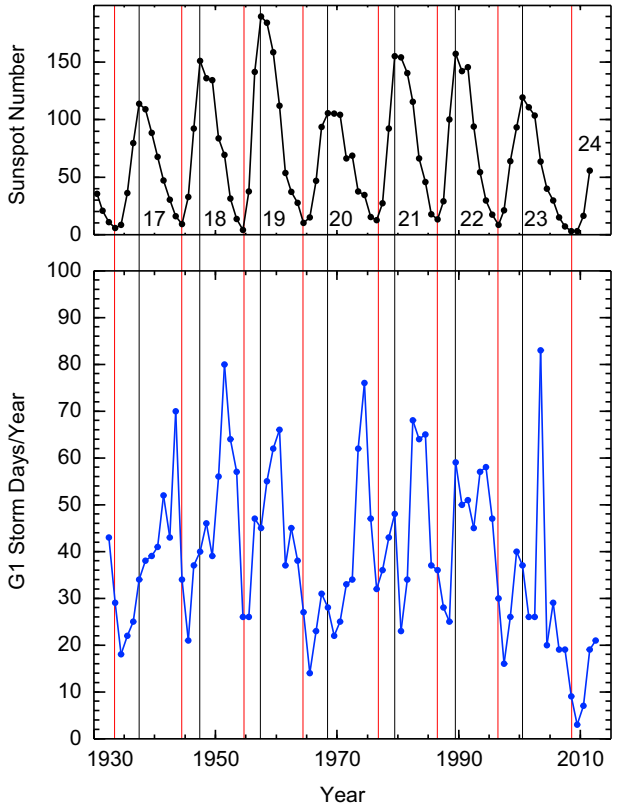

Fig. 1. Yearly mean SSN (top panel) and the number of NOAA G1 ("minor") storm days/year, from 1932 to 2012, encompassing the late phase of solar cycle 16 to the rise of cycle 24. The vertical red (black) lines indicate years of minimum (maximum) SSN in each cycle. The lowest rates during this period occurred in the minimum between cycles 23 and 24. The rate during the rise phase of cycle 24 is also lower than in any comparable interval during the period in this figure. Even 4 years into cycle 24, the storm rate is still only comparable to, or less than, the rates in the minimum activity years of previous cycles.

The G1 level corresponds to $5 \leq K_p < 6$. As noted by Richardson & Cane (2012b), the yearly G1 storm rates were lower in the minimum following cycle 23 than at any other time since 1932. In addition, it is evident from Figure 1 that the G1 storm rate continued to be lower than is typical during the rise phase of cycle 24. Remarkably, rates even 4 years into cycle 24 are still only comparable to those found in the quietest years since 1932.

To compare activity during the rise phases of the cycles shown in Figure 1, Figure 2 shows the yearly rates of NOAA G1, G2 ("moderate"; $6 \leq K_p < 7$), G3 ("strong"; $7 \leq K_p < 8$), and G4 ("severe"; $8 \leq K_p < 9$) storm days during the first 4 years after sunspot minimum for cycles 17–24, commencing at the month of minimum SSN (see Fig. 5 of Richardson & Cane 2012b for the $\geq$ G2 storm rates during the complete period in Fig. 1). The cycle number is indicated by the symbol type, with blue squares for cycle 24. Errors are calculated as the square root of the number of storm days. The G1 rate in cycle 24 clearly lies below the other cycles considered throughout the rise phase, with a particularly low level of storm activity during the first year of the cycle. By year 4, the G1 rate is around a third of that in the most active cycle (22). Another interesting feature to note is the drop in the cycle 21 (open orange squares) G1 storm rate in year 4, also seen for stronger storms. This is associated with the decrease in geomagnetic activity around the maximum of this cycle (cf. Fig. 1) that may be related to the "Gnevyshev gap" in energetic solar activity around the time of the solar magnetic field reversal near solar maximum (Gnevyshev 1967, 1977; Feminella & Storini 1997; Richardson et al. 2002a; Richardson & Cane 2012a). A similar, though typically less pronounced decrease in geomagnetic activity is found around the maximum of some other cycles (e.g., Richardson & Cane 2012a, 2012b, and references therein), and is evident for the larger (>G1) storms during year 4 of some of the other cycles in Figure 2.

Figure 3 compares the storm activity in cycles 17–24 using the *cumulative* year-by-year storm day rate for the first 4 years after smoothed sunspot minimum (i.e., the cumulative rate for the nth year is the sum of the yearly rates in years 1 to n). It is again clear that the storm rates in cycle 24 are substantially below those of any other cycle since cycle 17, especially for the weaker storms where the statistics are higher. (An exception is the G3 rate, which is comparable to that in cycle 17.) For example, the G1 rate in year 4 of cycle 24 is around a half that of the next lowest cycles (17, 20, and 23), which are also the weaker cycles in the top panel of Figure 1, and around a third of the highest rates observed, in cycles 19, 21, and 22, which are the strongest cycles. Note that the exceptionally low G1 storm rate in the first year of cycle 24 makes a significant contribution to the difference in the cumulative rates, but even taking this into consideration, the storm rate still rises less rapidly in cycle 24 than in the other cycles.

3. Relationship between storm rate and cycle peak SSN

To explore further the relationship between storm day rate and cycle size suggested by Figures 1 and 3, Figure 4 shows the cumulative G1, G2, or G3 storm rates in year 4 of cycles 17–23 plotted vs. the peak smoothed SSN in each cycle. This confirms a trend for the storm rates in the rise of the cycle to be correlated with the size of the cycle. Such a trend is not unexpected since geomagnetic activity has been used previously to predict the size of the developing sunspot cycle (e.g., Ohl 1966; Feynman 1982; Thompson 1993). (We note though that by year 4, cycles such as 21, with a minimum smoothed SSN in June 1976 and peak in December 1979, are already at or close to maximum so the cumulative storm rate in year 4 should not be considered as a "predictor" of the cycle size.) Extrapolating the cumulative G1 linear fit to the rate (50) observed in year 4 of cycle 24 would suggest a corresponding "peak SSN" of ~73 for this cycle. Similarly, the G2 and G3 fits and year 4 rates suggest peak SSNs of ~110 and ~95 respectively. We have also examined the correlation with peak SSN for the year 1–3 cumulative and yearly G1 to G3 storm rates. We find correlations with $cc > 0.75$ for the cumulative G1 rate in year 2 (leading to an inferred cycle 24 peak SSN ~65) and year 3 (peak cycle 24 SSN~84), the cumulative G2 rate in year 2 (peak cycle 24 SSN~99) and year 3 (peak cycle 24 SSN~97), the yearly G1 rate in year 2 (peak cycle 24 SSN~95) and year 3 (peak cycle SSN~108), the yearly G2 rate in year 2 (peak cycle 24 SSN~106), and the yearly G3 rate in year 3 (peak cycle 24 SSN~110). Figure 5 (from http://www.swpc.noaa.gov/SolarCycle/) illustrates the monthly SSN from January, 2000 to November, 2012, and the NOAA Space Weather Prediction Center prediction of the cycle development, which peaks at a SSN of 90 ± 10. The estimates inferred from the storm rates are reasonably consistent with this prediction, and suggest that cycle 24 will be the smallest cycle since at least cycle 17.

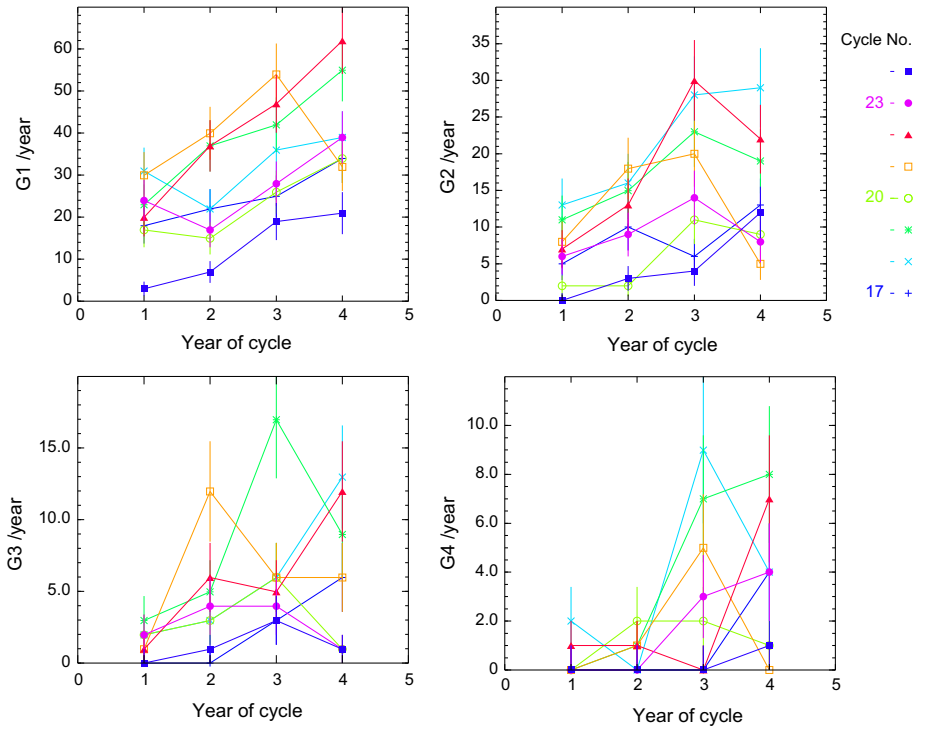

Fig. 2. Yearly rate of G1 to G4 storm days during the first 4 years of solar cycles 17–24; the symbol indicates the cycle number (blue squares for cycle 24). Error bars are given by the square root of the number of storm days. Note the tendency for the storm rate in year 4 to fall, associated with the decline in geomagnetic activity around solar maximum in the "Gnevyshev gap".

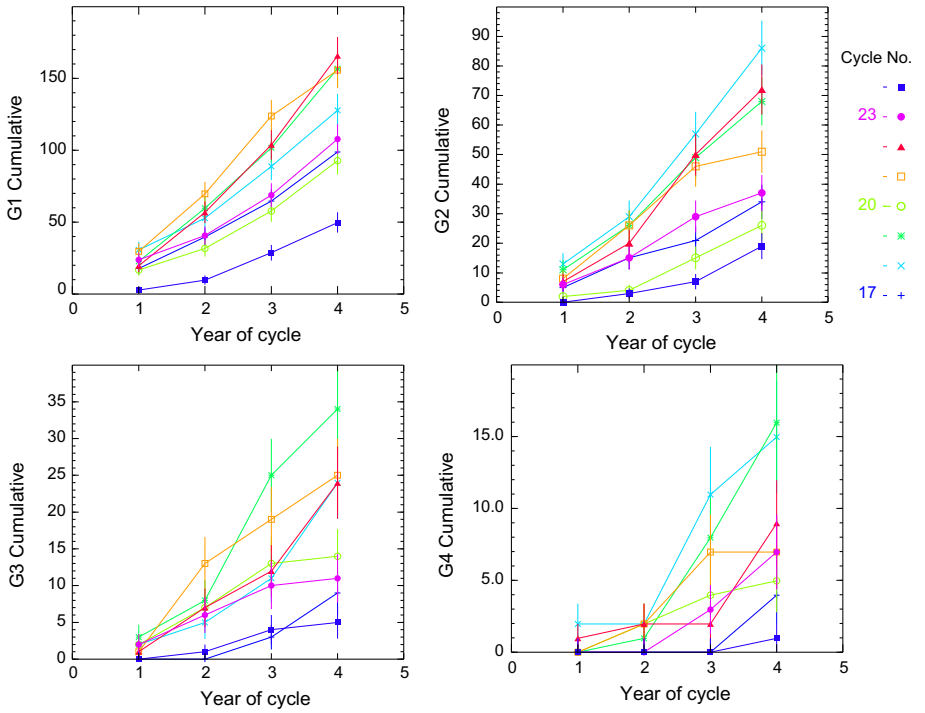

Fig. 3. Cumulative rate of G1 to G4 storm days during the first 4 years of solar cycles 17–24; the symbol indicates the cycle number. Error bars are given by the square root of the number of storm days. The storm rates during cycle 24 (blue squares) are clearly below those in the previous cycles, in particular for the weaker storms where there are better statistics. Note also that the rates for cycles 17, 20, and 23, the weaker cycles in Figure 1 tend to lie below those for the stronger cycles.

4. Contribution of ICME-associated structures and high-speed streams to the G1 and G2 storm rates

In Figure 1, comparison of the SSN and G1 storm rate suggests that the storm rate is not simply determined by solar activity levels. In particular, the rate tends to peak during the declining phase of each cycle when recurrent storms generated by corotating high-speed streams are particularly prominent (e.g., Bartels 1932, 1940; Sheeley et al. 1976, 1977; Tsurutani et al. 1995; Richardson & Cane 2012b; and references therein).

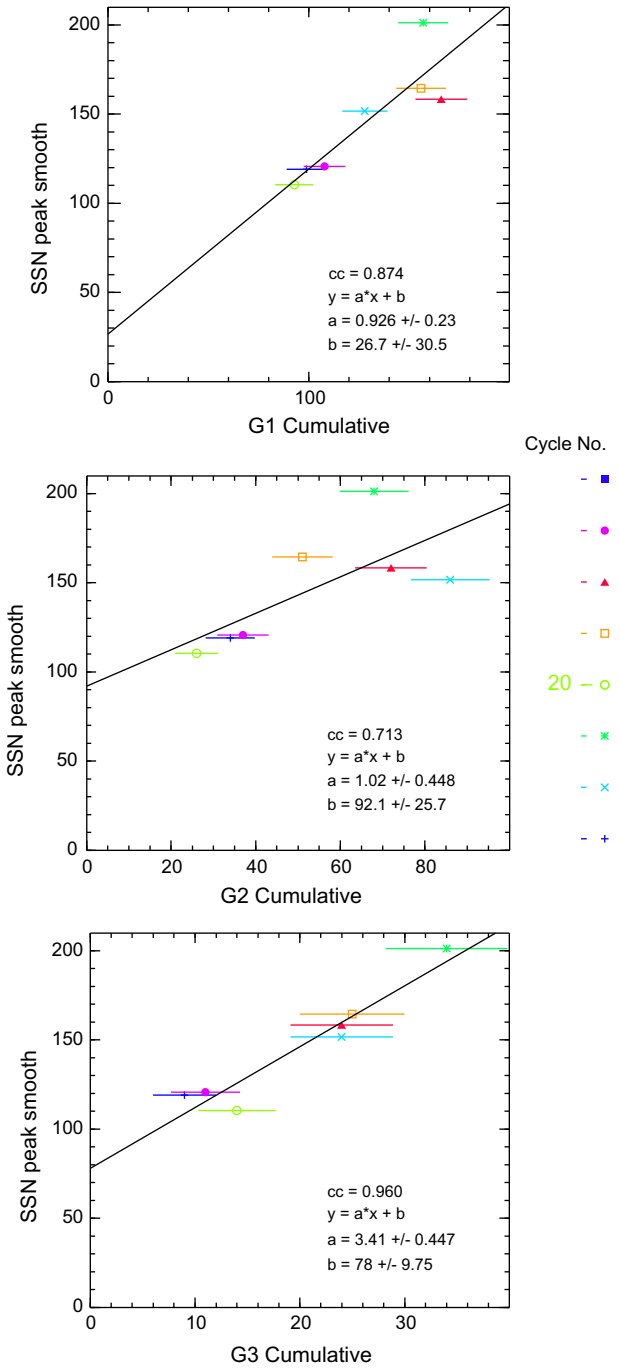

Fig. 4. Cumulative rate of G1, G2, and G3 storm days in the fourth years of solar cycles 17–23 plotted against the peak smoothed SSN in the same cycle. The symbol indicates the cycle number. Using the fitted lines and cumulative rates in cycle 24 suggests a peak SSN in cycle 24 of ~73 for the G1 rate, ~110 for G2, and ~95 for G3.

In Figure 6, we show the yearly rates of G1 and G2 storms (upper and lower rows, respectively) driven by ICMEs/sheaths (middle panels) and corotating streams (right-hand panels) during the first 4 years of cycles 20–24. The solar wind structure associations are inferred from the classification of solar wind flows based on the OMNI data set and additional data discussed in Richardson et al. (2000) and Richardson & Cane (2012a). The left-hand panels show the number of storms for which the structure type is uncertain, typically due to data gaps. For the G1 storms, the ICME/sheath-associated storm rate increases with the solar cycle, as might be expected, while the stream-associated rate is more variable from cycle to cycle, with no clear trend with time. Stream-associated storms make a substantial contribution to the total G1 storm rate that can be comparable to that from sheaths/ICMEs in years 3–4 and is dominant in earlier years. Note that the rates from both contributions are generally lower in cycle 24 than in previous cycles. The G2 storms show similar patterns, but clearly the contribution from corotating streams to these larger storms (~10%) is substantially lower than for G1 storms. Again the cycle 24 rates tend to lie below those for previous cycles. However, interestingly, the year 4 rate for sheath/ICME-associated storms in cycle 24 lies above those for all the cycles except 22, because of the decreases in these cycles associated with the Gnevyshev gap. This may be consistent with cycle 24 still being in the rising phase by the end of the fourth year of the cycle, whereas the other cycles have reached maximum. This would imply a longer cycle rise phase as expected for a smaller cycle due to the "Waldmeier effect" (Waldmeier 1935, 1939).

5. *Dst* index and geomagnetic storms

We now turn to consider the *Dst* ("disturbance storm time") index (Sugiura 1964). Figure 7 shows the *Dst* index during the first 4 years of cycles 20–24; *Dst* is available since 1957. "Intense" storm levels are indicated by $Dst < -100$ nT and "severe" by $Dst < -200$ nT (Tsurutani & Gonzalez 1997). Inspection of Figure 7 shows that severe storms were present during the first 4 years of each cycle except for cycle 24, and the occurrence of $Dst < -100$ nT was also much reduced in cycle 24. The latter point is illustrated in the bottom right panel of Figure 7 which shows the cumulative number of hours in the first 4 years of cycles 20–24 with $Dst < -100$ nT. This threshold was exceeded for only 61 h during the first 4 years of cycle 24 compared with 174 h in the next lowest cycle (20) and 530 h in cycle 22.

There were 10 intense storms and no severe storms during the first 4 years of cycle 24 compared with 21 intense and 4 severe storms in the same period of cycle 23 (e.g., Zhang et al. 2007; Echer et al. 2008). The cycle 24 storms are listed in Table 1. Inspecting the near-Earth solar wind observations for each of the intense storms, we find that all were associated with the passage of ICMEs and/or their related sheaths (in situ signatures of ICMEs are reviewed in Zurbuchen & Richardson 2006), and that in each case, the ICME had the enhanced magnetic fields and slow rotation in direction associated with a "magnetic cloud" (Klein & Burlaga 1982) suggestive of a flux-rope like magnetic field configuration. These storms only modestly exceeded the intense storm threshold, the strongest storm having minimum $Dst = -143$ nT. Note that the *Dst* values for the storms in 2012 are based on "quicklook" data and are may be subject to change, typically only by a few nT, when "provisional" or "final" values become available. Figure 8 shows solar wind observations (from the OMNI database; http://omniweb.gsfc.nasa.gov/) for the storm on July 15, 2012 that was driven by a magnetic cloud with a "unipolar" persistent southward (negative B_z) magnetic field suggesting that the magnetic cloud axis was highly inclined to the ecliptic.

6. Why was intense storm activity so low during the rise of cycle 24?

Previous studies (e.g., Gosling et al. 1991; Tsurutani & Gonzalez 1997; Zhang et al. 2007; Echer et al. 2008) have

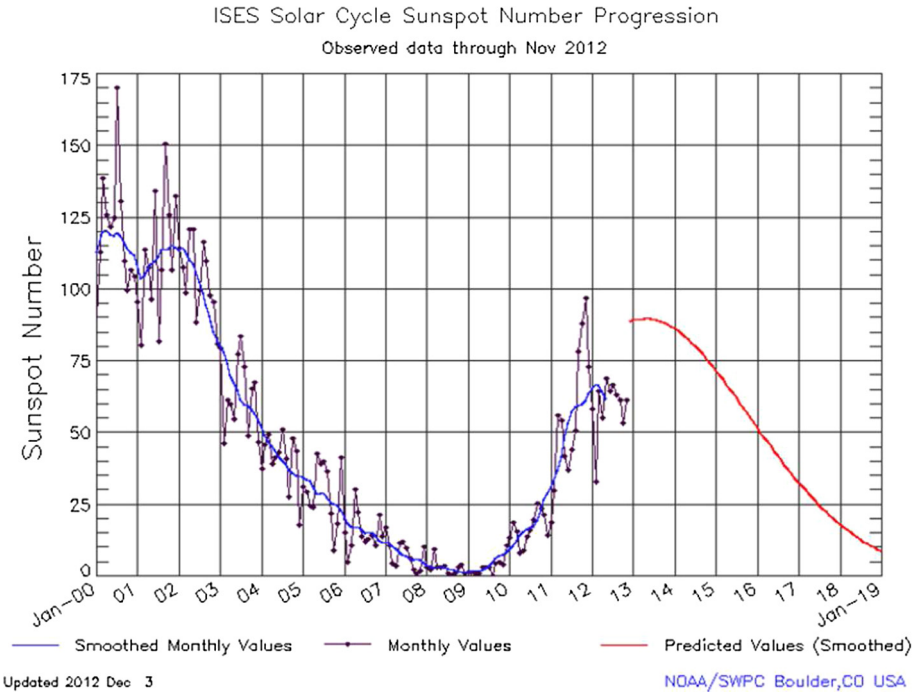

Fig. 5. Sunspot number from 2000, near the peak of cycle 23 to November 2012.

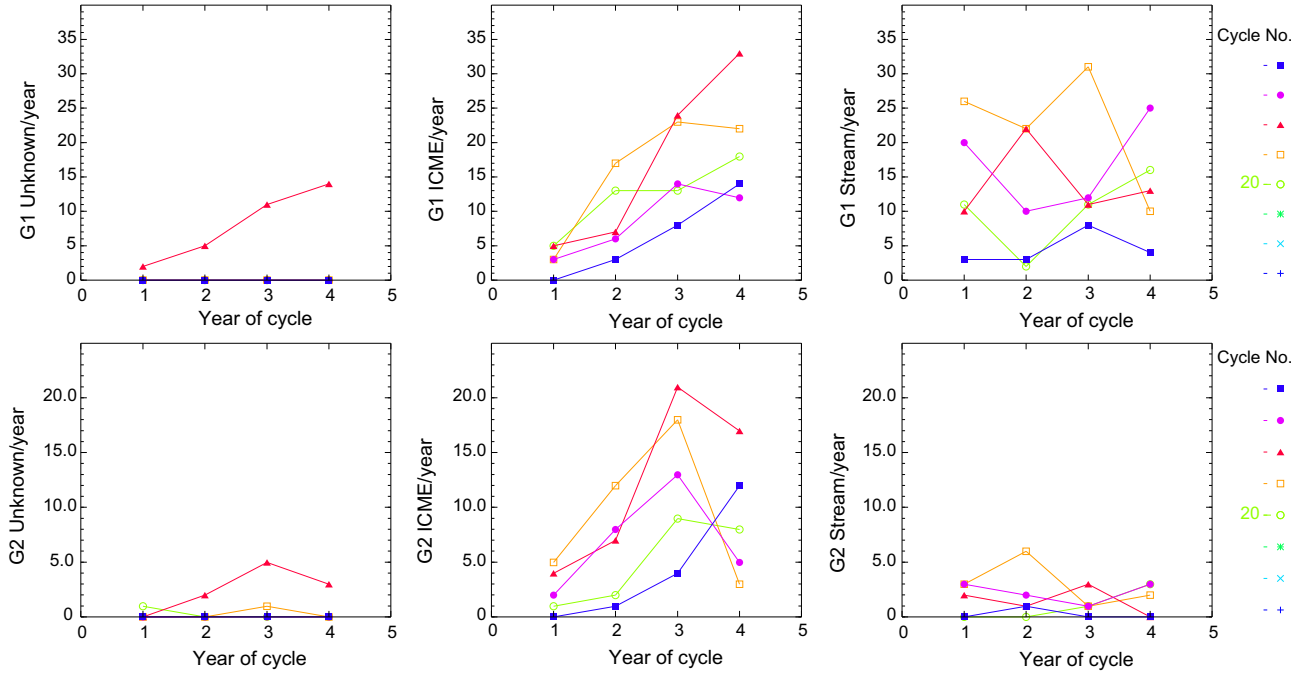

Fig. 6. Yearly number of G1 (upper row) and G2 (lower row) storms in the first 4 years of cycles 20–24 related to ICME-associated structures (middle panel in each row) and corotating high-speed streams (right panels), as inferred from solar wind flow classifications using the OMNI data set and additional data. The left-hand panels indicate the number of storms for which the structure is unknown. These are largely in cycle 22, when the solar wind data are from IMP 8 with significant gaps when the spacecraft was inside the Earth's bow shock.

demonstrated that intense ($Dst \leq 100$ nT) geomagnetic storms are predominantly associated with the passage of ICMEs and their upstream sheaths, or with corotating high-speed streams (cf., Table 1). For the $\geq$ intense storms in cycle 23, around 10% were associated with corotating streams, the remainder with ICMEs/sheaths (Zhang et al. 2007). Thus, to understand the causes of the low rate of intense storms in the rise phase of cycle 24, we focus on the properties of these structures.

As discussed in Section 1, geomagnetic activity is predominantly driven by the southward component of the magnetic field, and the solar wind speed, which combined are summarized by the y-component of the solar wind convective electric field $E = -V \times B$, i.e., $E_y \sim VB_s$; the Poynting flux for postive E_y and southward B in the solar wind is then directed into the magnetosphere. For example, the main (maximum) phase of the storm in Figure 8 was evidently driven by large values of E_y

Table 1. Geomagnetic storms with $Dst < -100$ nT during the first 4 years of solar cycle 24 (December, 2008 to November, 2012),

Year	Time of Dst_{min}	Dst_{min}	Driver
2009	No events	...	...
2010	No events	...	...
2011	August 6, 0300	−113 nT	Sheath
2011	September 26, 2300	−103 nT	Sheath
2011	October 25, 0100	−137 nT	Sheath
2012	March 9, 0800	−143 nT	Magnetic cloud
2012	April 24, 0400	−104 nT	Magnetic cloud
2012	July 15, 1800	−133 nT	Magnetic cloud
2012	October 1, 0300	−133 nT	Sheath + Magnetic cloud?
2012	October 8, 1200	−106 nT	Sheath
2012	October 9, 0800	−111 nT	Magnetic cloud
2012	November 14, 0700	−109 nT	Magnetic cloud

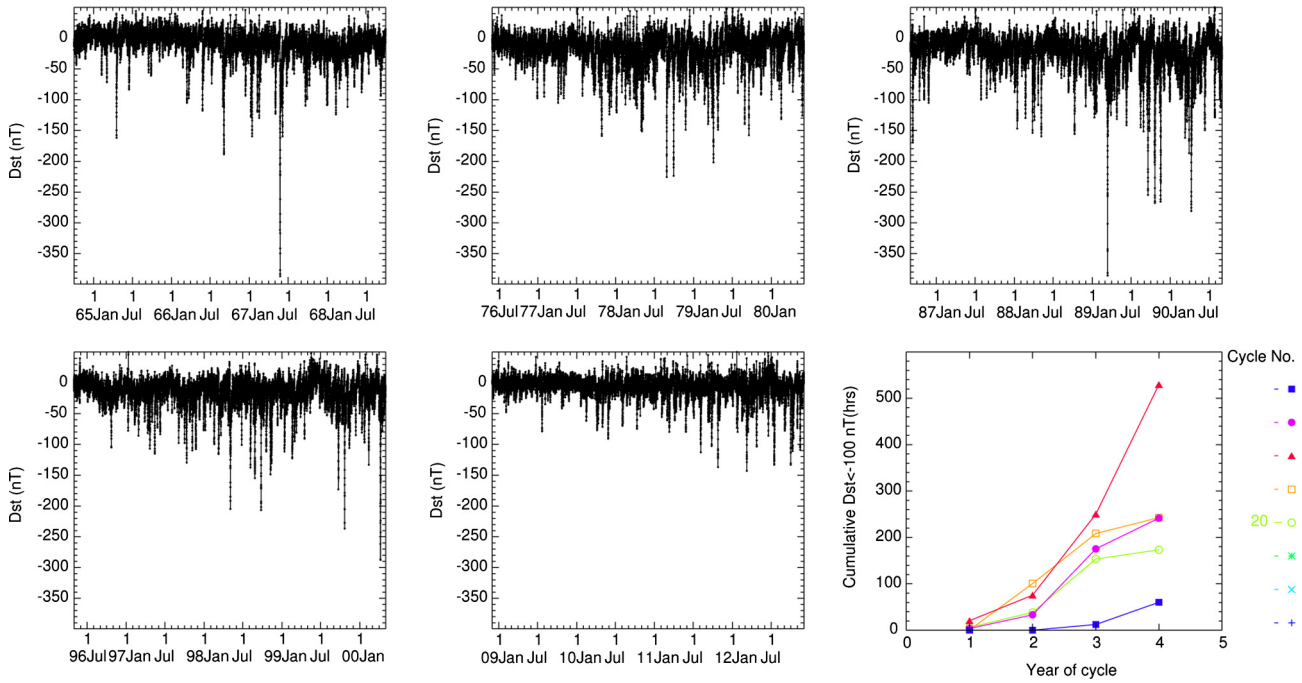

Fig. 7. *Dst* index during the first 4 years of solar cycles 20 to 24, and the cumulative number of hours in which $Dst < -100$ nT during these intervals. Note that no severe ($Dst < -200$ nT) storms occurred in the first 4 years of cycle 24 but were present in all the previous cycles shown.

and southward magnetic fields ($B_Z < 0$) inside the leading edge of the magnetic cloud. Figure 9 compares the minimum *Dst* with the maximum (one-hour averaged) value of E_y observed during the passage of ICMEs and the upstream sheath for ICMEs in the first 4 years of cycles 23 and 24. The ICMEs in this study are based on an updated version of the ICME catalog of Richardson & Cane (2010) that is available at the ACE Science Center (http://www.srl.caltech.edu/ACE/ASC/) or from the author. The first contributor to the lower geomagnetic activity levels in the rise phase of cycle 24 may be the 20% fewer ICMEs (86 vs. 106) observed at Earth compared to cycle 23, at least based on the catalog used in this study. (A few events are not plotted in Fig. 9 because *Dst* remained positive, or E_y is not available.) As is typical (e.g., Richardson & Cane 2010), the minimum *Dst* is anti-correlated with the maximum E_y in the ICME or sheath. Comparison of the results in Figure 9 suggests that the absence of the larger ($Dst < -150$ nT) ICME-driven storms in cycle 24 compared to cycle 23 was due to the lack of ICMEs/sheaths with large values ($\geq$ 10 mV/m) of E_y. Note however that the slope of the fitted line, and hence the *Dst* response to a given E_y, is similar in each cycle (-12.6 ± 0.7 nT/mV/m in cycle 23 and -13.6 ± 0.7 nT/mV/m in cycle 24).

Figure 10 shows similar plots of minimum *Dst* vs. maximum (1-h averaged) value of the southward magnetic field (when available) for ICMEs/sheaths in cycles 23 and 24. Again as is typical (e.g., Richardson & Cane 2010), minimum *Dst* and maximum B_s are also anti-correlated. The lack of the largest storms in cycle 24 is evidently associated with a general absence of ICMEs/sheaths with large (>15 nT) southward fields. In this case, however, the slope of the best fit line is different in cycles 23 and 24. Since the *Dst* response to E_y was similar in each cycle, the lower geoeffectiveness for a given value of B_s in cycle 24 suggests that the speeds of the ICMEs/sheaths were systematically lower than in cycle 23. The difference in the *Dst* – B_s slopes suggests a decrease in typical ICME speeds of ~20% in cycle 24. To examine the actual ICME speeds, Figure 11 shows the mean solar wind

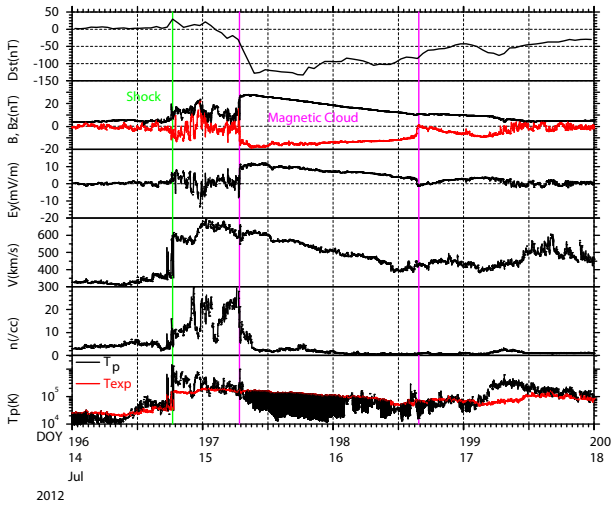

Fig. 8. The *Dst* index, and solar wind magnetic field (in GSE coordinates) and plasma parameters, for the July 15, 2012, geomagnetic storm with minimum *Dst* = −133 nT, associated with passage of a magnetic cloud with a southward magnetic field ($B_Z < 0$). The bottom panel shows the solar wind proton temperature (T_p, black) with the "expected" temperature (T_{exp}, red) superposed. T_{exp} is inferred from the T_p – solar wind speed relationship found in "normal" solar wind using the observed solar wind speed. The black shaded region indicates where $T_p \leq 0.5\ T_{exp}$, which is a frequent feature of magnetic clouds and other interplanetary coronal mass ejections (see Richardson & Cane 1995 for further details). OMNI 1-min solar wind data are shown; the fluctuations near shock passage are artifacts of the data mapping from the ACE spacecraft.

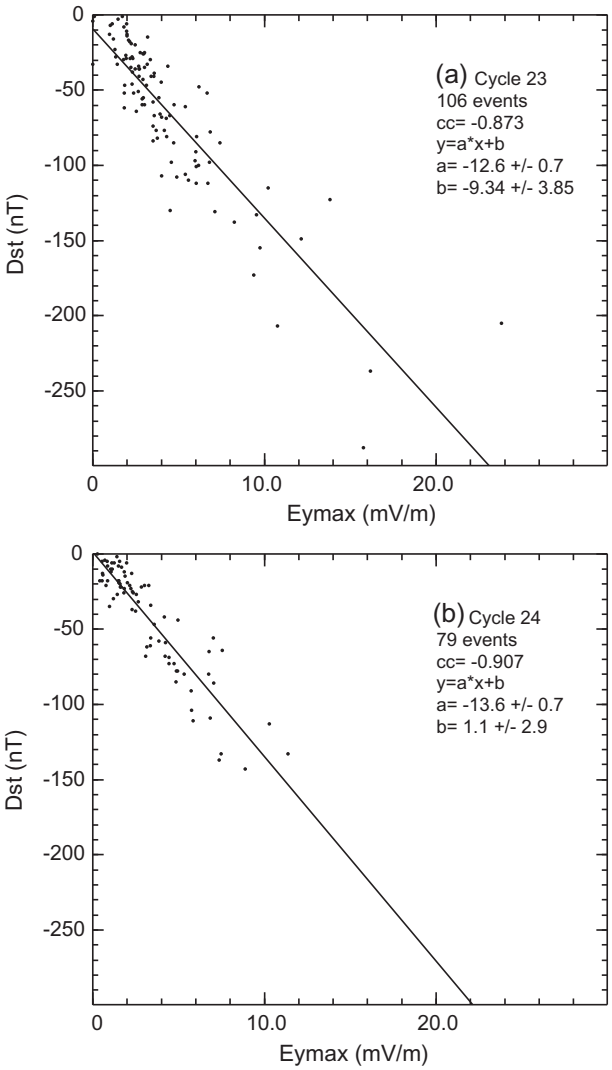

Fig. 9. Minimum *Dst* plotted vs. maximum E_y during the passage of ICMEs and the related sheaths during the first 4 years of cycles 23 and 24.

speeds in individual ICMEs in 1996–2012 (open circles) together with the mean ICME speeds (blue graph) and average solar wind speeds (red graph) in each year. The figure clearly illustrates how average ICME speeds tend to track average solar wind speeds, and that only a small subset of events have speeds that considerably exceed the average values. It is evident from Figure 11 that such events have been relatively absent in the rise of cycle 24 compared to cycle 23. For example, 18 ICMEs during the first 4 years of cycle 23 had mean speeds above 500 km/s compared with 8 in the equivalent period of cycle 24. Furthermore, while average ICME speeds typically exceeded average solar wind speeds in cycle 23, during the rise phase of cycle 24, average ICME and solar wind speeds have been more comparable. Thus in summary, the absence of large southward magnetic fields in sheaths/ICMEs and lower ICME speeds, which fewer exceptionally fast events, have reduced the geoeffectiveness of sheaths/ICMEs in cycle 24 compared to cycle 23.

Previous studies have noted that the tendency for the magnetic fields in "bipolar" magnetic clouds to be either southward in the leading half turning to northward in the trailing half (S-N) or vice versa (N-S) has a 22-year cycle and depends on the direction of the Sun's dipolar magnetic field (e.g., Bothmer & Schwenn 1998; Mulligan et al. 1998; Li & Luhmann 2004). In the rising phase of cycle 24, N-S clouds would be expected to be predominant, and this appears to be the case (Li et al. 2011; Kilpua et al. 2012). Zhang & Burlaga (1988) concluded that N-S clouds are typically less geoeffective than S-N clouds. Possible factors include: Activity that is initiated by southward fields in the sheath is likely to continue to grow in the case of a S-N cloud whereas a northward leading field will cut off the development of the storm (which may later re-intensify as the southward fields in the trailing half encounter the Earth); compression at the leading edge of the ICME due to interaction with the upstream sheath may enhance any southward fields present; and higher solar wind speeds inside the trailing edge than in the trailing half due to expansion of the ICME may also increase the geoeffectiveness of S-N clouds. We note though that Zhang & Burlaga (1988) actually attributed the difference in geoeffectiveness to the higher speeds of the S-N events in their sample, which were also more likely to be associated with shocks. More recently, Li & Luhmann (2004) and Kilpua et al. (2012) have concluded that the geoeffectiveness is similar for each type of cloud. In particular, Kilpua et al. (2012) found that the geoeffectiveness of the dominant N-S magnetic clouds during the rise of cycle 24 was frequently enhanced by the interaction with a high-speed stream trailing the magnetic cloud. Thus, the difference in the dominant bipolar cloud type may not be a major contributor to the difference in storm rates in the rise of cycles 23 and 24. For a more extensive discussion of the properties of magnetic clouds during these intervals, see Kilpua et al. (2012).

Notwithstanding the exceptionally low levels of geomagnetic activity and lack of severe storms during the rise phase of cycle 24, a caveat should be noted. On July 24, 2012, an

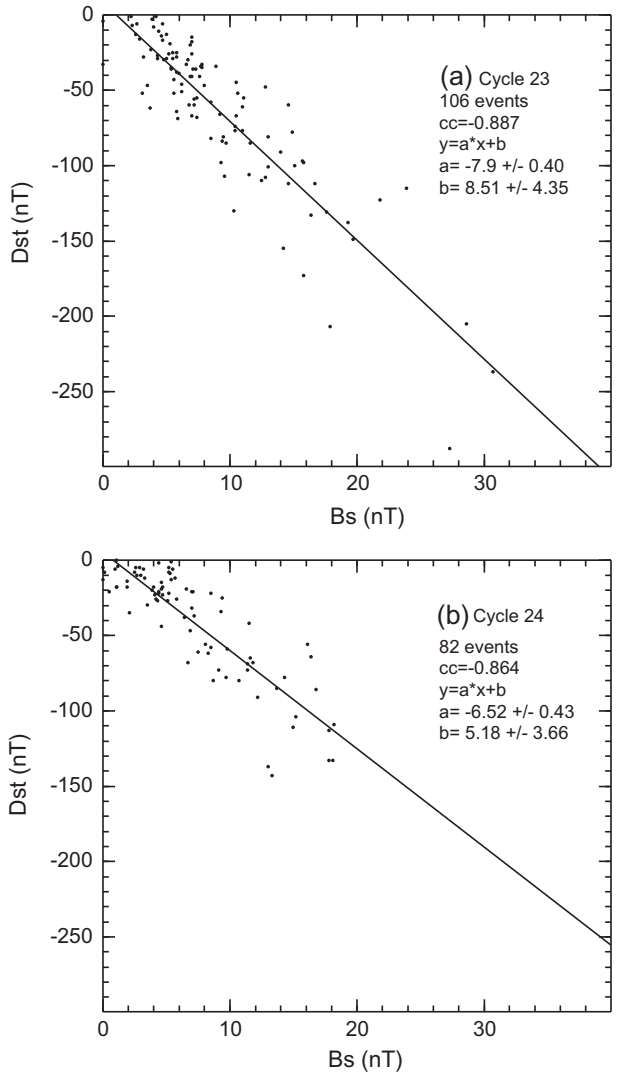

Fig. 10. Minimum *Dst* plotted vs. maximum B_S during the passage of ICMEs and the related sheaths during the first 4 years of cycles 23 and 24.

ICME with southward fields of ~45 nT encountered the STEREO A spacecraft when 140 West of Earth (see the *N* magnetic field component in Fig. 12). Had this ICME encountered Earth, then the fits in Figure 10 suggest that it would have resulted in a geomagnetic storm with minimum $Dst \sim -350$ or -290 nT depending on which of the two fits is assumed, or -370 nT using the $Dst - B_s$ relationship obtained for a larger sample of ICMEs by Richardson & Cane (2010). The more intense estimates are comparable to the largest storms observed during cycle 23. This example illustrates how the occurrence of the potentially destructive but rare geomagnetic storms is largely determined by chance; fortuitously, this ICME was not directed toward Earth. As noted by Richardson & Cane (2012b), the occurrence rate of the largest (G5) storms during cycles 17–23 has little correlation with the size of the sunspot cycle. Furthermore, Table 5 of Cliver & Svalgaard (2004) indicates that two of the largest geomagnetic storms since 1868 (based on the Aa^*_m index), on October 31, 1903 and September 25, 1909, occurred during solar cycle 17 (February, 1902 to August, 1913), which had a similar peak SSN (64) to cycle 24, at least based its current development. Thus, the unusually low levels of geomagnetic activity during the rise of cycle 24 do not mean that exceptionally strong storms are unlikely to occur in this cycle.

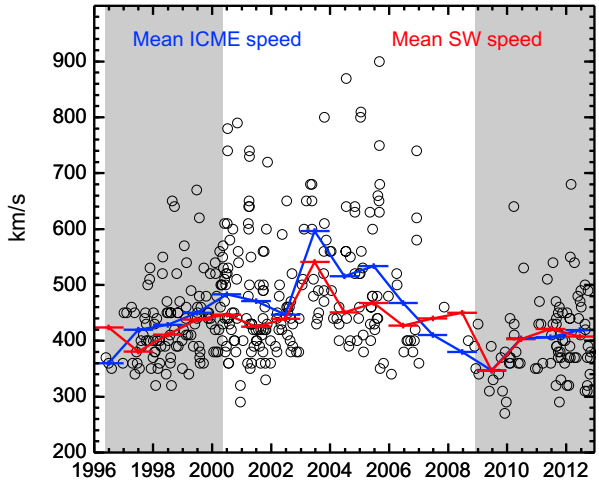

Fig. 11. Speeds of ICMEs observed in 1996–2012, including cycle 23 and the rise of cycle 24 with the yearly averaged ICME and solar wind speeds overlaid. Shaded regions indicate the first 4 years of each cycle. In the rise of cycle 23, the mean ICME speed is above the solar wind speed, and many ICMEs far exceed the mean solar wind speed. In cycle 24, the mean ICME and solar wind speeds are comparable, and few ICMEs have speeds much greater than the solar wind speed.

7. Geoeffectiveness of corotating streams

As discussed above, corotating high-speed streams also contribute to enhanced geomagnetic activity, as indicated specifically by their contribution to the G1 storm rate in Figure 6. This figure also illustrates that the rate of such storms was lower in the rise of cycle 24 than in other cycles since cycle 20, the earliest cycle when we can use in-situ observations to determine the storm drivers. We now briefly examine why this is the case. Figure 13 shows 3-solar rotations of the average magnetic field intensity in corotating streams, identified using the solar wind flow analysis discussed above, since 1963. As discussed by Richardson et al. (2002a), the field strength in streams tends to follow the well-known solar cycle variation in the IMF intensity. As has been previously noted (e.g., Smith & Balogh 2008; Connick et al. 2011), the IMF was at unusually low intensities, at least since the beginning of the space era, in the minimum following cycle 23, and this is reflected in the weak fields in high-speed streams in Figure 13. It is evident however, that the stream fields, though increasing, have continued to be at low levels during the rise of cycle 24, and 4 years into the cycle have barely reached the lowest levels detected since observations began. Geomagnetic activity associated with streams is typically associated with intermittent intervals of southward fields associated with large amplitude Alfvénic fluctuations (e.g., Burlaga & Lepping 1977; Tsurutani et al. 2006; and references therein). The weaker fields imply that such southward fields are also likely to be reduced during the rise of cycle 24, resulting in lower levels of geomagnetic activity associated with corotating streams. Solar wind speed is another factor to consider. However, Figure 11 suggests that mean solar wind speeds were comparable during the rise of cycles 23 and 24. Thus, we suggest that the smaller magnetic field strengths in corotating streams, that reflect the low intensities generally in the solar wind in the rise of cycle 24, are predominantly

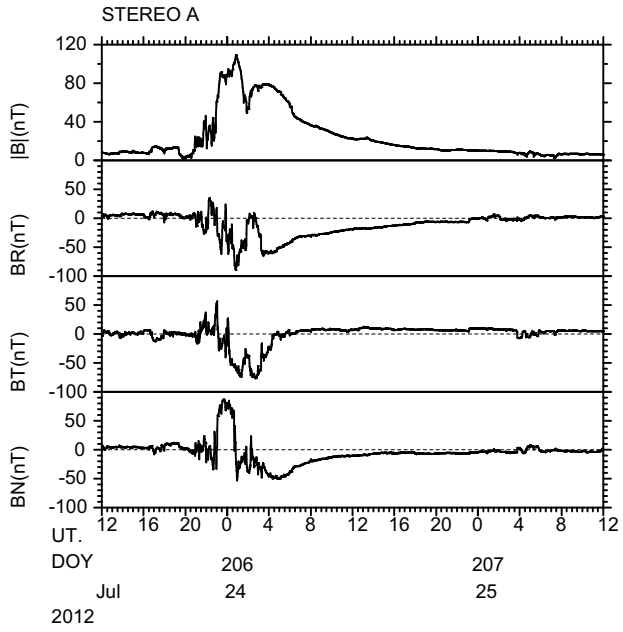

Fig. 12. Magnetic field observations (in RTN coordinates) during passage of the ICME observed by STEREO A on July 24, 2012. The southward (negative *N* component) magnetic fields reaching ~45 nT would have been highly geoeffective had the ICME encountered the Earth.

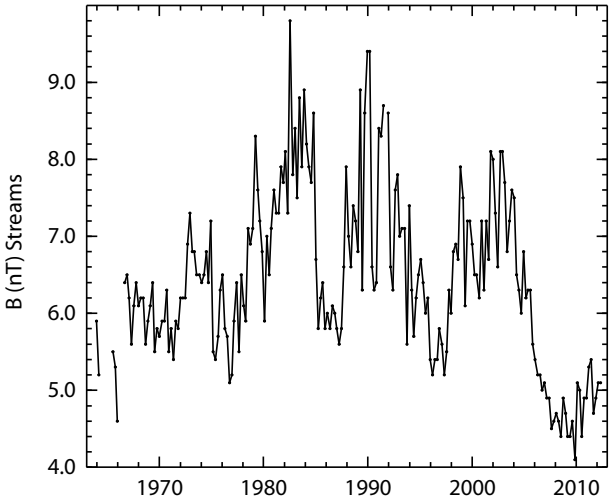

Fig. 13. Three-solar rotation averages of the magnetic field intensity in corotating streams in 1963–2012, showing the unusually weak fields present in the rise of cycle 24.

responsible for the low geoeffectivenes of corotating streams at this time.

8. Conclusions

The observations summarized in this paper demonstrate that:

- Geomagnetic activity levels during the rise phase (first 4 years) of solar cycle 24 were lower than during any comparable period since at least cycle 17, the earliest cycle that can be investigated using the K_p geomagnetic index.
- Even 4 years into cycle 24, G1 storm rates are still only comparable to or below the *minimum* rates seen in previous cycles.
- The rate of storm days (defined by the NOAA G storm sizes) during the rise phase of each cycle is approximately correlated with the peak SSN in the cycle. If this relationship can be extrapolated to the lower storm rates found in cycle 24, they suggest values for the peak SSN in cycle 24 that are consistent with the NOAA SWPC prediction, and indicate that cycle 24 is likely to be the weakest cycle since at least 1932.
- Both ICME- and stream-related storm activity were reduced in the rise of cycle 24 compared to cycles 20–23.
- No severe ($Dst < -200$ nT) storms were observed during the rise of cycle 24, whereas such storms were present in all the previous cycles since cycle 20, the earliest cycle with complete *Dst* data. There have been half as many intense ($Dst < -100$ nT) storms as in the similar period of cycle 23.
- An ICME observed at STEREO A in July 2012 with southward magnetic fields reaching ~45 nT might have produced an intense storm with minimum $Dst \sim -300$ nT had it instead encountered the Earth. Thus, the unusually weak levels of geomagnetic activity prevailing during the rise of solar cycle 24 do not also imply that exceptionally strong storms are unlikely to occur during this cycle.

Factors which may contribute to the lower levels of geomagnetic activity in cycle 24 include:

- ~20% fewer ICMEs passed Earth during the rise of cycle 24 compared to cycle 23, at least based on the updated Richardson & Cane (2010) catalog used in this study.
- A general absence of ICMEs/sheaths with large values of E_y (> 10 mV/m) that would typically give rise to major geomagnetic storms. This is the result of a combination of a lack of such structures with strong southward magnetic fields (> 20 nT) and fewer ICMEs with speeds exceeding average solar wind speeds compared with cycle 23.
- The predominance of N-S magnetic clouds might be expected to contribute, but as noted by Kilpua et al. (2012), they were often trailed by high-speed streams which increased their geoeffectiveness.
- Weaker fields in corotating streams compared with cycle 23.

Acknowledgements. We thank the many investigators that have contributed to the near-Earth solar wind observations that have allowed the solar wind drivers of geomagnetic activity to be determined. The geomagnetic data were obtained from the US National Geophysical Data Center and the World Data Center for Geomagnetism, Kyoto. The STEREO data are from the IMPACT-MAG instrument, P.I. Janet Luhmann. We thank Bruce Tsurutani for comments on the presentation at the American Geophysical Union 2012 Fall meeting on which this paper is based.

References

Arnoldy, R.L., Signature in the interplanetary medium for substorms, *J. Geophys. Res.*, **76**, 5189, DOI: 10.1029/JA076i022p05189, 1971.

Bartels, J., Terrestrial magnetic activity and its relation to solar phenomena, *Terr. Magn. Atmos. Elect.*, **37**, 1, 1932.

Bartels, J., Solar activity and geomagnetism, *Terr. Magn. Atmos. Elect.*, **45**, 339, 1940.

Bothmer, V., and R. Schwenn, The structure and origin of magnetic clouds in the solar wind, *Ann. Geophys.*, **16**, 1, 1998.

Burlaga, L.F., and R.P. Lepping, The causes of recurrent geomagnetic storms, *Planet. Space Sci.*, **25**, 1151, 1977.

Cliver, E.W., and L. Svalgaard, The 1859 solar-terrestrial disturbance and the current limits of extreme space weather activity, *Sol. Phys.*, **224**, 407, 10.1007/s11207-005-4980-z, 2004.

Connick, D.E., C.W. Smith, and N.A. Schwadron, Interplanetary magnetic flux depletion during protracted solar minima, *Astrophys. J.*, **727**, 8, DOI: 10.1088/0004-637X/727/1/8, 2011.

Dungey, J.W., Interplanetary magnetic field and the auroral zones, *Phys. Rev. Lett.*, **6**, 47, 1961.

Echer, E., W.D. Gonzalez, B.T. Tsurutani, and A.L.C. Gonzalez, Interplanetary conditions causing intense geomagnetic storms ($Dst \leq -100$ nT) during solar cycle 23 (1996–2006), *J. Geophys. Res.*, **113**, A05221, DOI: 10.1029/2007JA012744, 2008.

Feminella, F., and M. Storini, Large scale dynamical phenomena during solar activity cycles, *A&A*, **322**, 311, 1997.

Feynman, J., and N.U. Crooker, The solar wind at the turn of the century, *Nature*, **275**, 626, 1978.

Feynman, J., Geomagnetic and solar wind cycles, 1900–1975, *J. Geophys. Res.*, **87**, 6153, 1982.

Gnevyshev, M.N., On the 11-years cycle of solar activity, *Sol. Phys.*, **1**, 107, 1967.

Gnevyshev, M.N., Essential features of the 11 year solar cycle, *Sol. Phys.*, **51**, 175, 1977.

Gosling, J.T., D.J. McComas, J.L. Phillips, and S.J. Bame, Geomagnetic activity associated with Earth passage of interplanetary shock disturbances and coronal mass ejections, *J. Geophys. Res.*, **96**, 7831, 1991.

Hirshberg, J., and D.S. Colburn, Interplanetary field and geomagnetic variations: A unified view, *Planet. Space Sci.*, **17**, 1183, DOI: 10.1016/0032-0633(69)90010-5, 1969.

Ji, E.-Y., Y.-J. Moon, and K.-H. Kim, Statistical comparison of interplanetary conditions causing intense geomagnetic storms ($Dst \leq -100$ nT), *J. Geophys. Res.*, **115**, A10232, DOI: 10.1029/2009JA015112, 2010.

Kilpua, E.K.J., Y. Li, J.G. Luhmann, L.K. Jian, and C.T. Russell, On the relationship between magnetic cloud field polarity and geoeffectiveness, *Ann. Geophys.*, **30**, 1037, 2012.

Klein, L.W., and L.F. Burlaga, Interplanetary magnetic clouds at 1 AU, *J. Geophys. Res.*, **87**, 613, 1982.

Li, Y., and J.G. Luhmann, Solar cycle control of the magnetic cloud polarity and the geoeffectiveness, *J. Atmos. Solar-Terr. Phys.*, **66**, 323, 2004.

Li, Y., J.G. Luhmann, B.J. Lynch, and E.K.J. Kilpua, Cyclic reversal of magnetic cloud poloidal field, *Sol. Phys.*, **270**, 331, 2011.

Menvielle, M., and A. Berthelier, The K-derived planetary indices: Description and availability, *Rev. Geophys.*, **29**, 415, DOI: 10.1029/91RG00994, 1991.

Mulligan, T., C.T. Russell, and J.G. Luhmann, Solar cycle evolution of the structure of magnetic clouds in the inner heliosphere, *Geophys. Res. Lett.*, **25**, 2959, 1998.

O'Brien, T.P., and R.L. McPherron, An empirical phase space analysis of ring current dynamics: solar wind control of injection and decay, *J. Geophys. Res.*, **105**, 7707, 2000.

Ohl, A.I., Forecast of sunspot maximum of cycle 20, *Solice Danie*, **9**, 84, 1966.

Perrealt, P., and S.-I. Akasofu, A study of geomagnetic storms, *Geophys. J. R. Astron. Soc.*, **54**, 547, 1978.

Richardson, I.G., and H.V. Cane, Regions of abnormally low proton temperature in the solar wind (1965–1991) and their association with ejecta, *J. Geophys. Res.*, **100**, 23397, 1995.

Richardson, I.G., and H.V. Cane, Near-Earth interplanetary coronal mass ejections during solar cycle 23 (1996–2009): catalog and summary of properties, *Sol. Phys.*, **264**, 189, 2010.

Richardson, I.G., and H.V. Cane, Near-earth solar wind flows and related geomagnetic activity during more than four solar cycles (1963–2011), *J. Space Weather Space Clim.*, **2**, A02, DOI: 10.1051/swsc/2012003, 2012a.

Richardson, I.G., and H.V. Cane, Solar wind drivers of geomagnetic storms during more than four solar cycles, *J. Space Weather Space Clim.*, **2**, A01, DOI: 10.1051/swsc/2012001, 2012b.

Richardson, I.G., E.W. Cliver, and H.V. Cane, Sources of geomagnetic activity over the solar cycle: Relative importance of CMEs, high-speed streams, and slow solar wind, *J. Geophys. Res.*, **105 (18)**, 203, 2000.

Richardson, I.G., H.V. Cane, and E.W. Cliver, Sources of geomagnetic activity during nearly three solar cycles (1972–2000), *J. Geophys. Res.*, **107**, DOI: 10.1029/2001JA000504, 2002a.

Richardson, I.G., E.W. Cliver, and H.V. Cane, Long-term trends in interplanetary magnetic field strength and solar wind structure during the twentieth century, *J. Geophys. Res.*, **107**, DOI: 10.1029/2001JA000507, 2002b.

Russell, C.T., On the possibility of deducing interplanetary and solar parameters from geomagnetic records, *Sol. Phys.*, **42**, 259, 1975.

Russell, C.T., J.G. Luhmann, and L.K. Jian, How unprecedented a solar minimum?, *Rev. Geophys.*, **48**, RG2004, DOI: 10.1029/2009RG000316, 2010.

Sheeley Jr., N.R., J.W. Harvey, and W.C. Feldman, Coronal holes, solar wind streams, and recurrent geomagnetic disturbances, 1973–1976, *Sol. Phys.*, **49**, 271, 1976.

Sheeley Jr., N.R., J.S. Asbridge, S.J. Bame, and J.W. Harvey, A pictorial comparison of interplanetary magnetic field polarity, solar wind speed, and geomagnetic disturbance index during the sunspot cycle, *Sol. Phys.*, **52**, 485, 1977.

Smith, E.J., and A. Balogh, Decrease in heliospheric magnetic flux in this solar minimum: recent Ulysses magnetic field observations, *Geophys. Res. Lett.*, **35**, L22103, DOI: 10.1029/2008GL035345, 2008.

Stamper, R., M. Lockwood, M.N. Wild, and T.D.G. Clark, Solar causes of the long-term increase in geomagnetic activity, *J. Geophys. Res.*, **104**, 28–325, 1999.

Sugiura, M., Hourly values of equatorial *Dst* for the IGY, *Ann. Int. Geophys. Year*, **35**, 9, 1964.

Svalgaard, L., and E.W. Cliver, Heliospheric magnetic field 1835–2009, *J. Geophys. Res.*, **115**, A09111, DOI: 10.1029/2009JA015069, 2010.

Thompson, R.J., A technique for predicting the amplitude of the solar cycle, *Sol. Phys.*, **148**, 383, 1993.

Tsurutani, B.T., and W.D. Gonzalez, The interplanetary causes of magnetic storms: a review. in : *A.G.U. Geophys. Monogr. Ser.*, edited by B.T., Tsurutani, W.D. Gonzalez, Y. Kamide, and J.K. Arballo, **Vol. 98**, AGU, Washington, DC, 77, 1997.

Tsurutani, B.T., W.D. Gonzalez, A.L.C. Gonzalez, F. Tang, J.K. Araballo, and M. Okada, Interplanetary origin of geomagnetic activity in the declining phase of the solar cycle, *J. Geophys. Res.*, **100(21)**, 717, 1995.

Tsurutani, B.T., N. Gopalswamy, R.L. McPherron, W.D. Gonzalez, G. Lu, and F.L. Guarnieri, Magnetic storms caused by corotating solar wind steams. in *Recurrent Magnetic Storms: Corotating Solar Wind Streams*, edited by B.T., Tsurutani, et al., A.G.U. Geophysical Monograph, **167**, 45, 2006.

Tsurutani, B.T., E. Echer, and W.D. Gonzalez, The solar and interplanetary causes of the recent minimum in geomagnetic activity (MGA23): a combination of midlatitude small coronal holes, low IMF B_Z variances, low solar wind speeds and low solar magnetic fields, *Ann. Geophys.*, **29**, 839, DOI: 10.5194/angeo-29-839-2011, 2011.

Waldmeier, M., Neue Eigenschaften der Sonnenfleckenkurve, *Astron. Mitt. Zurich*, **14 (133)**, 105, 1935.

Waldmeier, M., Die Zonenwanderung der Sonnenflecken, *Astron. Mitt. Zurich*, **14 (138)**, 470, 1939.

Zhang, G., and L.F. Burlaga, Magnetic clouds, geomagnetic disturbances and cosmic ray decreases, *J. Geophys. Res.*, **93**, 2511, 1988.

Zhang, J., I.G. Richardson, D.F. Webb, N. Gopalswamy, E. Huttunen, et al., Solar and interplanetary sources of major geomagnetic storms ($Dst \leq -100$ nT) during 1996–2005, *J. Geophys. Res.*, **112**, A12105, DOI: 10.1029/2007JA012332, 2007.

Zurbuchen, T.H., and I.G. Richardson, In-situ solar wind and magnetic field signatures of interplanetary coronal mass ejections, *Space Sci. Rev.*, **123**, 31–34, 2006.

Cite this article as: Richardson IG: Geomagnetic activity during the rising phase of solar cycle 24. J. Space Weather Space Clim., 2013, **3**, A08.